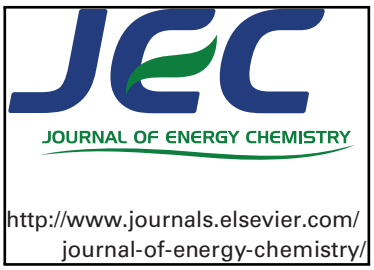

Application of phenonaphthazine derivatives as hole-transporting materials for perovskite solar cells

Xueyuan Liu , Fei Zhang , Xicheng Liu , Mengna Sun ,
Shirong Wang , Dongmei Li , Qingbo Meng , Xianggao Li

PII: S2095-4956(16)30042-0
DOI: 10.1016/j.jechem.2016.03.021
Reference: JECHEM 151

To appear in: *Journal of Energy Chemistry*

Received date: 31 January 2016
Revised date: 5 March 2016
Accepted date: 14 March 2016

Please cite this article as: Xueyuan Liu , Fei Zhang , Xicheng Liu , Mengna Sun , Shirong Wang , Dongmei Li , Qingbo Meng , Xianggao Li , Application of phenonaphthazine derivatives as hole-transporting materials for perovskite solar cells, *Journal of Energy Chemistry* (2016), doi: 10.1016/j.jechem.2016.03.021

Graphical abstract

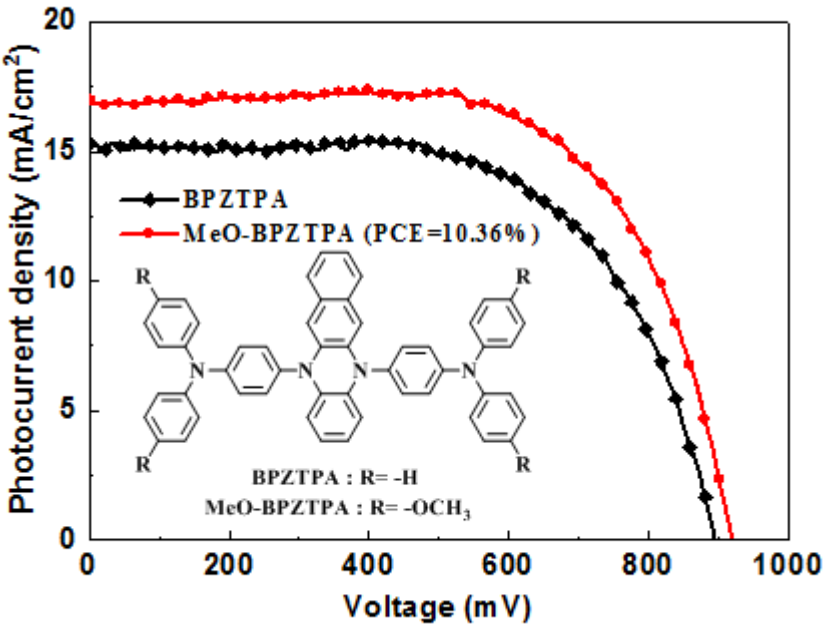

Application of phenonaphthazine derivatives as hole-transporting materials for perovskite solar cells

Xueyuan Liu[a,b], Fei Zhang[a,b], Xicheng Liu[a,b], Mengna Sun[a,b], Shirong Wang[a,b], Dongmei Li[c,*], Qingbo Meng[c], Xianggao Li[a,b,*]

[a] *School of Chemical Engineering and Technology, Tianjin University, Tianjin 300354, China*

[b] *Collaborative Innovation Center of Chemical Science and Engineering, Tianjin 300072, China*

[c] *Beijing Key Laboratory for New Energy Materials and Devices; Key Laboratory for Renewable Energy (CAS); Institute of Physics, Chinese Academy of Sciences, Beijing 100190, China*

Article history:

Received 31 January 2016

Revised 5 March 2016

Accepted 14 March 2016

Available online

Abstract: Two electron-rich, solution-processable phenonaphthazine derivatives, 5,12-bis{*N*-[4,4′-bis-(phenyl)-aminophen-4″-yl]}-phenonaphthazine (BPZTPA) and 5,12-bis{*N*-[4,4′-bis(methoxy-phenyl)aminophen-4″-yl]}-phenonaphthazine (MeO-BPZTPA) have been designed and employed in the fabrication of perovskite solar cells. BPZTPA and MeO-BPZTPA exhibit excellent thermal stabilities, hole mobilities (~10^{-4} $cm^2/(V·s)$) and suitable HOMO levels (-5.34 and -5.29 eV, respectively) relative to the valence band of the $CH_3NH_3PbI_3$ and Au work function, showing their potential as alternative hole-transporting materials (HTMs). Meanwhile, the corresponding mesoporous TiO_2/$CH_3NH_3PbI_3$/HTM/Au devices are investigated, and the best power conversion efficiency of 10.36% has been achieved for MeO-BPZTPA without using *p*-type dopant.

Keywords: Perovskite solar cell; Phenonaphthazine; Hole-transporting material; Triphenylamine derivatives

*** Corresponding author.** Tel: +86-22-27404208; E-mail: lixianggao@tju.edu.cn (Xianggao Li);
Tel: +86-10-82649242; E-mail: dmli@ipcy.ac.cn (Dongmei Li).

1. Introduction

Perovskite solar cells (PSCs) have shown tremendous advancement in power conversion efficiency (PCE) starting from 3.8% to 20.2%, comparable to conventional inorganic solar cells (i.e. CdTe, CIGS) [1─4]. In PSCs, hole-transporting layer plays a key role in facilitating hole transportation from perovskite to the electrode and inhibiting back electron transfer as well [5]. 2,2′,7,7′-Tetrakis(*N*,*N*′-di-*p*-methoxy-phenylamine)-9,9′-spirobifluorene (*spiro*-OMeTAD) has been widely used as the hole-transporting materials (HTMs) for efficient PSCs, however, its expensive price and uncertain stability are challenges for the PSCs' future. Recently, different kinds of HTMs have been developed, including inorganic HTMs, polymeric HTMs and small molecular HTMs. Inorganic HTMs (CuI and CuSCN) have drawn much attention due to their high hole mobilities and low production cost [2]. Organic HTMs appear to be good candidates for PSCs. Polymeric HTMs, such as conjugated PTAA (polytriarylamine) [4], DR3TBDTT [6], have also shown the competitive performances in PSCs. However,

small molecular HTMs have advantages of their convenient purification, controllable molecular structures and relatively high efficiency [7]. Such HTMs including DOR3T-TBDT [8], DMFA-FA [9] and PST1 [3] etc., have shown PCEs more than 13%. From a commercialization viewpoint, these compounds deserve extensive investigation to reduce the high cost of PSCs.

As an important type of organic HTMs, triphenylamine (TPA) derivatives not only have the advantages of high hole mobility and good thermal stability, but also their energy levels can be adjusted reasonably by changing the molecular structure. To date, many TPA-based HTMs for PSCs have been widely reported [10─13]. For example, Mhaisalkar and Grimsdale fabricated the PSCs with HTMs containing thiophene core with TPA side groups, presenting 15.4% PCE [14]. Li and Meng reported a series of HTMs containing TPA moiety for PSCs with PCEs over 11% [5,15─18].

Encouraged by these reports, we developed two alternative HTMs with phenonaphthazine core and TPA side groups, namely BPZTPA and MeO-BPZTPA, which were prepared using a simple C─N coupling reaction versus the widely used *spiro*-OMeTAD. The molecular structures and synthetic route for the HTMs are depicted in Scheme 1. The introduction of electron-rich phenonaphthazine unit is to adjust their HOMO levels to match well with that of perovskite and Au. On the other hand, the symmetrical structure is expected to enhance π-π stacking interactions, which could be beneficial for high hole mobility and enhancing the lifetime of a charge-separated excited state [19]. In this work, 10.36% of PCE has been achieved for the device with MeO-BPZTPA.

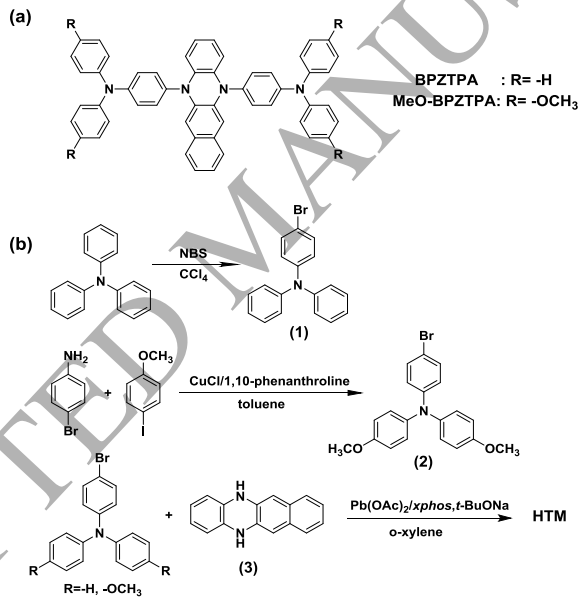

Scheme 1. (a) Molecular structures of BPZTPA and MeO-BPZTPA, (b) synthetic route for BPZTPA and MeO-BPZTPA.

2. Experimental

2.1. Materials

Starting materials were all available commercially and used without further purification if not mentioned specially. PbI_2 was obtained from Sigma-Aldrich. Hydroiodic acid (AR, 45 wt% in water) and methylamine (AR, 27% in methanol) were purchased from Sinopharm Chemical Reagent Co. Ltd. Sodium *tert*-butoxide (*t*-BuONa) was supplied by Aladdin. *N*,*N*′-dimethylformamide (DMF) and chlorobenzene are got from Alfar Aesar. *Spiro*-OMeTAD was obtained from Luminescence Technology Corp. 2-dicyclohexylphosphino-2′,4′,6′-trisopro -pylbiphenyl (*xphos*) was purchased from Beijing HWRK Chem Co. Palladium acetate, *p*-bromoaniline, 4-methoxyiodobenzene, triphenylamine, 2,3-Dihydroxynaphthalene and *o*-phenylenediamine were got from

Tianjin Xiensi Biochemical technology Co.LTD. Other reagents were supplied by Tianjin Guangfu Fine Chemical Research Institute, such as *N*-Bromosuccinimide (NBS), 1,10-phenanthroline, cuprous chloride and *o*-xylene. $CH_3NH_3I_3$ were synthesized according to literatures [20].

2.2. Measurements

^1H and ^{13}C NMR spectra were recorded with an INOVA 400 MHz spectrometer (Varian, USA) and AVANCE III 600 MHz spectrometer (Bruker, Switzerland). Mass spectra (MS) were performed on a Autoflex tof/tof III mass spectrometer (Bruker, Germany). UV-Visible spectra of the HTMs in tetrahydrofuran (THF) solutions (1×10^{-5} mol/L) were recorded with Thermo Evolution 300 UV-Vis spectrometer (Thermo Electron, USA) in the 200─800 nm wavelength range at room temperature. Thermo gravimetrical analyses (TGA) were recorded with TA Q500 thermo gravimetric apparatus (TA Instruments, USA) at a heating rate of 10 °C/min under nitrogen atmosphere. Differential scanning calorimetry (DSC) was conducted on TA Q20 Instrument (TA Instruments, USA) at a heating rate of 10 °C/min under nitrogen atmosphere. Photoemission yield spectroscopy (PYS) instrument was PYS-202 ionization energy test system (Sumitomo Heavy Industries, Japan) at the voltage of 100 V, waiting time of 1 s and energy range from 4.0 to 8.5 eV. The time-of-flight (TOF) measurements were performed on TOF401 (Sumitomo Heavy Industries. Ltd. Japan), for which the samples were prepared through spin coating using a structure ITO/HTM (about 1 μm)/Al (150 nm) with an active area of 3×10 mm^2. Surface morphology of the $TiO_2/CH_3NH_3PbI_3$/HTM/Au film was obtained using a scanning electron microscope (SEM, XL30S-FEG, FEI, USA). The film thickness was performed on a surface profiler (P-6, KLA-Tencor, USA).

2.3. Synthesis of HTMs

***N,N′*-diphenyl-4-bromoaniline (1):** Triphenylamine (7.41 g, 30.00 mmol) and NBS (5.61 g, 31.50 mmol) were dissolved in 80 mL CCl_4. The solution was heated to reflux for 5 h. The precipitated succinimide was filtered while hot, and the solvent was evaporated from the solution, getting light yellow oil. After recrystallization from dry ethanol, the desired product was obtained as a white powder, yielding 6.81 g (70%). Mp: 103─106 °C. ^1H NMR (600 MHz, $CDCl_3$) δ: 7.35─7.29 (m, 2H), 7.24 (d, *J* = 7.6 Hz, 4H), 7.06 (d, *J* = 8.1 Hz, 4H), 7.04─6.96 (m, 2H), 6.93 (dd, *J* = 10.7, 3.7 Hz, 2H).

(4-Bromo-phenyl)-di-*p*-methoxyaniline (2): In a 500 mL four-necked flask equipped with a mechanical stirrer, thermometer and water segregator, all under an argon atmosphere, 4-methoxyiodobenzene (29.30 g, 125.00 mmol), *p*-bromoaniline (8.60 g, 50.00 mmol) and 1,10-phenanthroline (1.80 g, 10.00 mmol) were added. 300 mL toluene was added and the reaction mixture was then heated to 100 °C, at which point potassium hydroxide flake (22.40 g, 400.00 mmol) and cuprous chloride (1.00 g, 10.00 mmol) were added. Then the mixture was heated to reflux for 12 h. The mixture was cooled to room temperature and extracted with ethyl acetate. The organic phase was combined and dried by $MgSO_4$. After filtrating the $MgSO_4$ and removing the solvent by reduced pressure distillation, the residue was purified by column chromatography on silicagel eluting with petroleum ether to give white product 11.41 g (59%). ^1H NMR (400 MHz, $CDCl_3$) δ: 7.27─7.17 (m, 2H), 7.03 (d, *J* = 8.7 Hz, 4H), 6.80 (dd, *J* = 12.2, 8.8 Hz, 6H), 3.79 (s, 6H); ^{13}C NMR (100 MHz, $CDCl_3$) δ: 156.08, 147.94, 140.58, 131.78, 126.59, 122.00, 114.81, 112.38, 55.50.

Phenonaphthazine (3): 2,3-dihydroxynapthalene (10.00 g, 62.50 mmol) and 1,2-phenylenediamine (6.75 g, 62.50 mmol) were placed into a round bottom flask under nitrogen atmosphere. 60 mL *N,N′*-dimethylaniline was added and mixture was heated to reflux for 4 h. After cooling to room temperature, suitable toluene was added and solid was collected by vacuum filtration. After washing with ethanol (100 mL) and hexane (50 mL) repeatedly, the product was dried under vacuum to yield 9.20 g (64%) of light yellow lamellar crystal. ^1H NMR (400 MHz, DMSO) δ: 8.11 (s, 2H), 7.16 (dd, *J* = 5.9, 3.3 Hz, 2H), 6.90 (s, 2H), 6.34 (s, 2H), 6.23 (s, 2H), 6.17 (s, 2H). ^{13}C NMR (100 MHz, DMSO) δ: 134.95, 132.88, 131.25, 125.23, 123.26, 120.64, 112.13, 104.72.

BPZTPA: Phenonaphthazine (0.93 g, 4.00 mmol), *N*,*N*′-diphenyl-4-bromoaniline (2.85 g, 8.80 mmol), *t*-BuONa (0.96 g, 10.00 mmol), *xphos* (0.26 g, 0.50 mmol) and *o*-xylene (120 mL) were all placed into a round bottom flask under a nitrogen atmosphere. After the mixture was dissolved, palladium acetate (0.03 g, 0.14 mmol) was added into flask quickly. Then mixture was heated to reflux for 6 h. When cooled to room temperature and added 200 mL water, the reaction liquid was extracted ethyl acetate. The organic phase was combined and dried by $MgSO_4$, leaving brown sticky liquid. After removing the solvent by reduced pressure distillation, the residue was purified by column chromatography on silicagel eluting with CH_2Cl_2:petroleum ether (1:6) to give yellow product 1.40 g (49%). ^{1}H NMR (400 MHz, DMSO) δ 7.59 (s, 2H), 7.39 (d, *J* = 6.7 Hz, 6H), 7.32 (s, 4H), 7.21 (d, *J* = 7.0 Hz, 6H), 7.13 (d, *J* = 7.2 Hz, 6H), 7.06 (s, 4H), 7.00 (s, 2H), 6.85 (s, 2H), 6.42 (s, 2H), 5.76 (s, 4H). MS (MALDI-TOF): *m*/z calcd for $C_{52}H_{38}N_4$: 718.31 [M^-]; found [M^-] 718.29.

MeO-BPZTPA: MeO-BPZTPA was obtained from phenonaphthazine and (4-bromo-phenyl)-di-*p*-methoxyaniline by following the same procedure as that used to make BPZTPA, giving yellow solid (43%). The residue was purified by column chromatography on silicagel eluting with CH_2Cl_2:petroleum ether (1:2). ^{1}H NMR (400 MHz, DMSO) δ: 7.19 (t, *J* = 7.5 Hz, 12H), 7.10 (d, *J* = 3.2 Hz, 2H), 6.97 (t, *J* = 9.8 *Hz*, 12H), 6.93 (d, *J* = 5.5 Hz, 2H), 6.36 (d, *J* = 3.4 Hz, 2H), 5.84 (s, 2H), 5.74 (dd, *J* = 5.5, 3.5 Hz, 2H), 3.75 (d, *J* = 8.6 Hz, 12H). MS (MALDI-TOF): *m*/z calcd for $C_{56}H_{46}N_4O_4$: 838.35 [M^-]; found [M^-] 838.35.

2.4. Solar cell fabrication

Substrates were fluorine-doped tin oxide conducting glass (FTO, Pilkington, thickness 2.2 mm, sheet resistance 14 Ω/square). Before used, patterned FTO glass was cleaned with mild detergent, rinsed with distilled water for several times and subsequently with ethanol in an ultrasonic bath, finally dried under air stream. For fabricating the device, TiO_2 compact layer and mesoporous TiO_2 layer were deposited on FTO glass in turn as reported [21]. And the $CH_3NH_3PbI_3$ perovskite film was subsequently deposited on the mesoporous TiO_2 film by using a modified two-step method according to the literatures [22]. For a deposition of HTM layer, BPZTPA or MeO-BPZTPA in chlorobenzene solution was prepared. HTMs were spin-coated on the mesoporous TiO_2/$CH_3NH_3PbI_3$ film at 2500 rpm for 30 s, and finally an 80 nm-thickness Au layer (Sigma-Aldrich) was deposited on the top of the HTM layer by thermal evaporation under 10^{-6} torr vacuum conditions.

2.5. Device measurement

For current density-voltage (*J-V*) characteristics, the cells were illuminated under 100 mW/cm^2 (AM 1.5G) by an Oriel solar simulator 91160A calibrated with a standard Si reference cell (National Institute of Metrology, China), and the *J-V* characteristics of the cells were recorded on Keithley 2602 SourceMeter. A mask with a window of 0.10 cm^2 was clipped to define the active area of the cell. The monochromatic incident photon-to-electron conversion efficiency (IPCE) spectrum was obtained on a lab-made IPCE testing system [5]. Electrochemical impedance spectra (EIS) of the perovskite solar cells were determined by a ZAHNER IM6e electrochemical workstation (Zahner, Germany) in the dark in the frequency ranging from 0.1 to 10^5 Hz at the applied bias voltage from 400 to 950 mV with a perturbation amplitude of 10 mV. The obtained impedance spectra were fitted with *Zview* software based on an appropriate equivalent circuit.

3. Results and discussion

3.1. Physical property of the HTMs

The UV-Vis absorption spectra of BPZTPA and MeO-BPZTPA in THF solution and in thin film state are shown in Figure 1(a), and the corresponding data are summarized in Table 1. The absorption spectra of their spin-coating thin films are significantly broadened and red-shifted with 7 nm in comparison to that of solution state

due to stronger intermolecular π-π stacking in the film [23].

The thermal properties of BPZTPA and MeO-BPZTPA are determined by the thermo gravimetric analysis (TGA, †ESI Fig. S5) and differential scanning calorimetry (DSC, †ESI Fig. S6) which are listed in Table 1. HTMs have high decomposition temperatures (T_d, 375.3 °C for BPZTPA and 308.2 °C for MeO-BPZTPA) and glass transition temperatures (T_g, 137.2 °C for BPZTPA and 141.2 °C for MeO-BPZTPA). This result reveals that these two HTMs have excellent thermal stability to favor their practical application in solar cells.

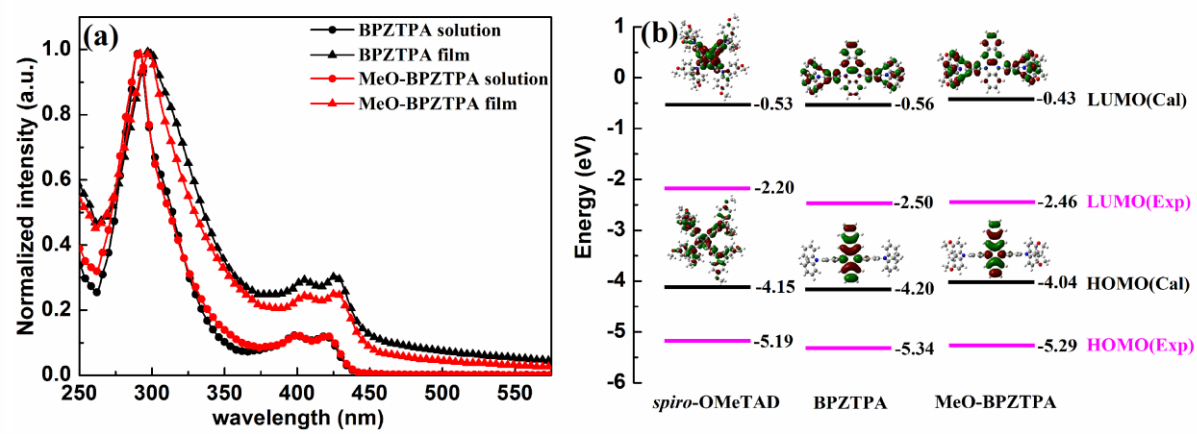

Figure 1. (a) UV-Vis absorption of solution in THF and films of BPZTPA and MeO-BPZTPA, (b) calculated and experimental energy levels and electronic density distributions of *spiro*-OMeTAD and BPZTPA, MeO-BPZTPA.

Table 1. Key physical data of BPZTPA and MeO-BPZTPA.

	λ_{abs} (nm)	λ_{onset} (nm)	E_g (eV)	HOMO (eV)	LUMO (eV)	T_m (ºC)	T_d (ºC)	T_g (ºC)	μ^e ($cm^2/(V\cdot s)$)
BPZTPA	292, 399, 419 /299[a], 405[a], 426[a]	447[a]	2.77[b] 3.64[d]	–5.34[c] –4.20[d]	–2.57[c] –0.56[d]	298.0	375.3	137.2	2.53×10^{-4}
MeO-BPZTPA	292, 400, 420 /299[a], 407[a], 427[a]	448[a]	2.77[b] 3.61[d]	–5.29[c] –4.04[d]	–2.52[c] –0.43[d]	–	308.2	141.2	4.80×10^{-4}
spiro-OMeTAD	310[a], 380[a]	421[a]	2.95[b] 3.62[d]	– 5.19[c] – 4.15[d]	– 2.24[c] – 0.53[d]	–	–	–	2.00×10^{-4}

[a] UV-Vis absorption of the films; [b] $E_g = 1240/\lambda_{onset}$; [c] experiment values (HOMO levels is measured by PYS; LUMO = HOMO + E_g); [d] theoretical calculation values by DFT (E_g = LUMO─HOMO); ─: not detected; thermal characteristics is measured by TGA and DSC; [e] Electric field : 1.8×10^5 V/cm.

To PSCs, upon excitation, electrons and holes are produced in the perovskite. The excited electrons are injected into the conduct band (CB) of TiO_2, then transferred through the TiO_2 and collected by the conducting substrate. Meanwhile, the holes in the valence band (VB) of the perovskite would transfer into the hole-transport layer. Thus, it requires that the HOMO levels of HTMs are matched more with those of the perovskite and Au work function [24]. The VBs of $CH_3NH_3PbI_3$ and Au work function are ─5.43 and ─5.1 eV respectively, which suggest that appropriate HOMO levels of HTMs are between ─5.43 and ─5.1 eV [21]. As we all know, *spiro*-OMeTAD as HTM has a very suitable HOMO level in perovskite solar cells.

To investigate the potential application of the two compounds as HTMs in hybrid perovskite solar cells, density functional theory (DFT) calculation via the Gaussian 03 program at the B3LYP/6-31G* level has been employed to predict optoelectronic properties of BPZTPA and MeO-BPZTPA, from which we learn that their calculations are very similar with that of calculated *spiro*-OMeTAD, indicating the HOMO levels of two HTMs

match well with $CH_3NH_3PbI_3$ and Au. The calculated frontier molecular orbitals of three compounds are shown in Figure 1(b). There is a completely difference on HOMO energy level distribution between two new HTMs and *spiro*-OMeTAD, while it is the same at the partial wave function overlap between LUMO and HOMO, leading to a strong Coulomb interaction and could favor formation of neutral excitons and hole transport [12].

Furthermore, their energy levels are experimentally measured by photoemission yield spectroscopy (PYS) (†ESI Fig. S7). The HOMO levels of BPZTPA and MeO-BPZTPA are determined to be −5.34 and −5.29 eV, which well match with those of $CH_3NH_3PbI_3$ and Au work function and are favorable for photogenerated carriers dissociation and charge transfer at the interfaces. Moreover, the optical band gap (E_g) is calculated from the absorption onset wavelength ($E_g = 1240/\lambda_{onset}$) of the corresponding absorption spectrum, indicating that the E_g are all 2.77 eV for BPZTPA and MeO-BPZTPA. The LUMO levels of HTMs are calculated to be −2.57 and −2.52 eV, which are more positive than that of $CH_3NH_3PbI_3$ (−3.92 eV). Thus, these two HTMs are supposed to not only act as a hole transporting layer, but also play as an electron blocking layer in the PSCs, leading to the reduction of electron from perovskite layer and hole from hole-transporting layer [21].

To understand the charge-carrier transport properties of BPZTPA and MeO-BPZTPA, their hole mobilities are evaluated by time-of-flight (TOF) measurement (†ESI Fig. S8). At room temperature, the hole mobilities of BPZTPA and MeO-BPZTPA are 2.53×10^{-4} and 4.80×10^{-4} $cm^2/(V \cdot s)$ at the electric field of 1.8×10^5 V/cm, respectively, both of which are higher than that of *spiro*-OMeTAD (2.00×10^{-4} $cm^2/(V \cdot s)$). They are thus supposed to exhibit good photovoltaic performance for perovskite solar cells.

3.2. Performance of the devices

3.2.1. Photovoltaic performance

The doping-free perovskite solar cells based on BPZTPA and MeO-BPZTPA as HTM are fabricated. The device structure (Figure 2a) and cross-sectional scanning electron microscopy (SEM) image (Figure 2b) of the perovskite solar cells are shown. The clear interfaces in the device structure and the cell composition of a 400 nm-thickness TiO_2 layer infiltrated with $CH_3NH_3PbI_3$, 300 nm-thickness $CH_3NH_3PbI_3$ capping layer and 80 nm-thickness Au electrode can be observed. In order to clearly show the HTM layer in the SEM image, 60 mg/mL of HTM chlorobenzene solution is adopted, which gives about 100 nm-thickness HTM film.

The current density-voltage (*J*-*V*) characteristics of the devices employing BPZTPA and MeO-BPZTPA are shown in Figure 2(c). And the corresponding photovoltaic parameters are summarized in Table 2. As we can see, the MeO-BPZTPA based cell present a PCE of 10.36% with a short-circuit current density (J_{sc}) of 16.89 mA/cm^2, an open-circuit voltage (V_{oc}) of 917.1 mV, and a fill factor (FF) of 0.669. However, the BPZTPA based cells only present a PCE of 8.52%. For comparison, the PSCs based on dopant-free *spiro*-OMeTAD (†ESI Fig. S9) is fabricated under the similar condition, exhibiting a PCE of only 3.55%. As expected, devices based on dopant-free BPZTPA and MeO-BPZTPA with higher hole mobilities exhibit much better photovoltaic performance than that with dopant-free *spiro*-OMeTAD , especially in terms of FF and J_{sc}. And the PSC without HTM is also fabricated, which J_{sc} is 12.47 mA/cm^2, V_{oc} is 843.9 mV and FF is 0.673, yielding a PCE of only 7.09%. Besides, the cell performance of the devices based on these two HTMs are still lower than that of the device with conventional doped *spiro*-OMeTAD, whose PCE is 13.65% with the J_{sc} of 19.17 mA/cm^2, V_{oc} of 1011.6 mV and FF of 0.704 (†ESI Fig. S9).

At the same time, the incident-photon-to-current conversion efficiency (IPCE) spectra of PSCs based on BPZTPA and MeO-BPZTPA as HTMs are given in Figure 2(d). Similar shapes of two IPCE spectra can be clearly observed, indicating that the HTM absorption has negligible effect on the cell performance under the premise of the same perovskite film fabrication process. Integral photocurrents from the overlap of the IPCE spectra are 14.22 mA/cm^2 for BPZTPA and 14.72 mA/cm^2 for MeO-BPZTPA, basically in agreement with the experimentally

obtained J_{sc} (Table 2). In PSCs, the V_{oc} depends on the difference between the HOMO level of HTM and the quasi-Fermi level of TiO_2 [25]. But there is no evident difference in open circuit voltage for BPZTPA and MeO-BPZTPA, resulting from their similar HOMO levels [26]. The device based on MeO-BPZTPA obtains a higher FF, which is on account of a better coverage of MeO-BPZTPA layer for its better solubility in organic solvents [6]. However, under the same fabrication condition, the device based on LiTFSI-doping MeO-BPZTPA did not exhibit the improvement in the cell performance, which J_{sc} is 18.28 mA/cm^2, V_{oc} is 927.6 mV and FF is 0.571, yielding a PCE of 9.69%, especially in the lower FF, therefore, all the following discussion is based on undoped HTMs. Further investigation about the effects of different dopants and optimization of doping process are still needed in our future work.

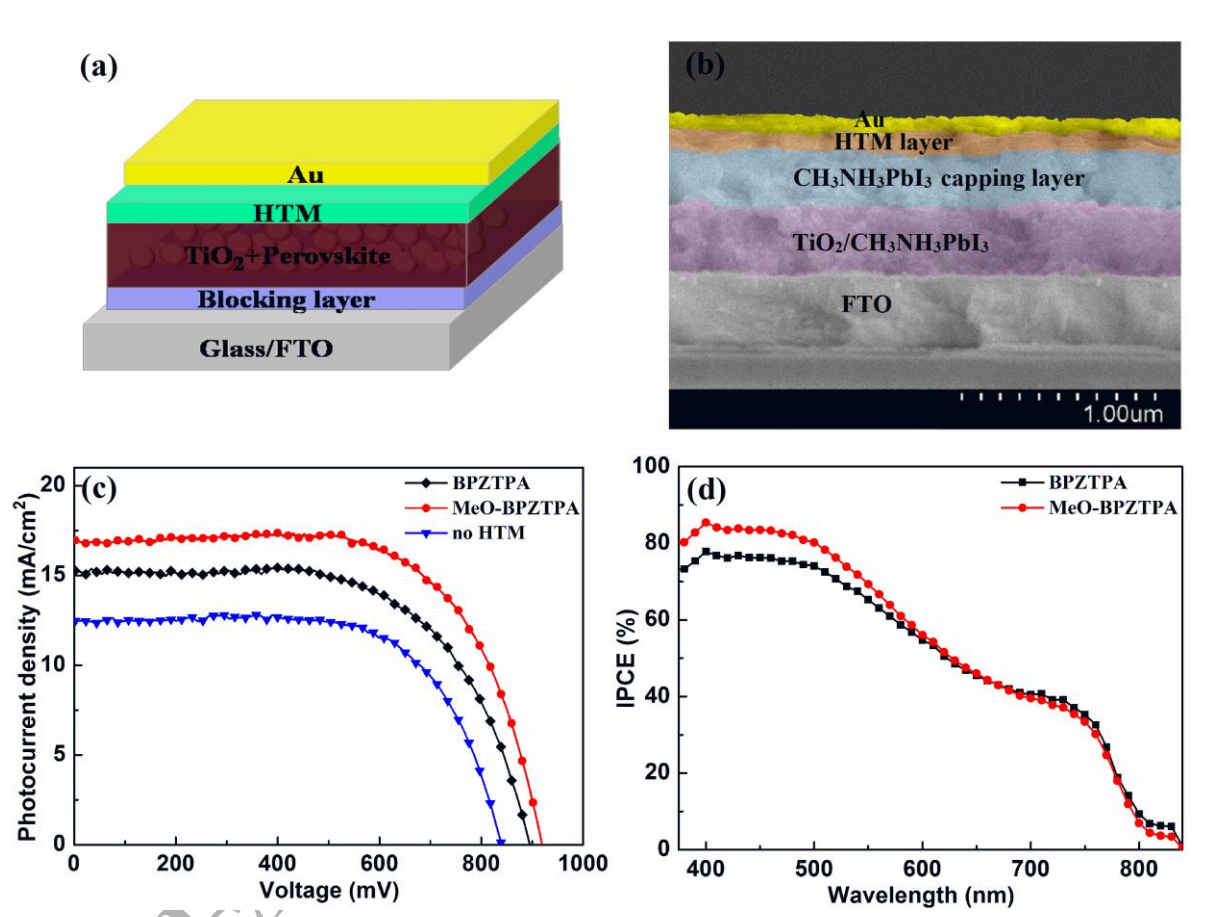

Figure 2. (a) Diagrammatic representation of photovoltaic device structure, (b) cross-sectional SEM image of the representative device, (c) *J-V* curves for the perovskite solar cells fabricated with BPZTPA, MeO-BPZTPA and without HTM, (d) IPCE spectrum of the cell with BPZTPA, MeO-BPZTPA.

In addition, the relationship between the J_{sc} of the solar cell with two HTMs and different light intensities is investigated, as shown in Figure 3(a). Good linear relation is observed, indicating that the charge collection ability of BPZTPA and MeO-BPZTPA in the perovskite solar cell is independent of light density. According to previous investigations, it can be inferred that no space-charge limited photocurrent occurs in the devices with two HTMs because of their high enough electron and hole mobilities [15].

Table 2. Device parameters of the devices with HTMs and no HTM.

HTM	J_{sc} (mA/cm^2)	V_{oc} (mV)	FF	PCE (%)
Dopant-free BPZTPA	15.29	896.2	0.621	8.52
Dopant-free MeO-BPZTPA	16.89	917.1	0.669	10.36
Dopant-free *spiro*-OMeTAD	13.27	887.4	0.287	3.55
Doped *spiro*-OMeTAD	19.17	1011.6	0.704	13.65
no HTM	12.47	843.9	0.673	7.09

Illumination : 100 mW/cm^2 simulated AM 1.5 G solar light; the effective area of device is 0.10 cm^2; HTM concentration: 10 mg/mL (BPZTPA and MeO-BPZTPA); 80 mg/mL (*spiro*-OMeTAD).

3.2.2. Electrochemical impedance spectra (EIS) measurement

In order to analyze the interfacial electron transfer and recombination processes, the EIS analysis is carried out. Nyquist plots in the dark over different forward biases of BPZTPA and MeO-BPZTPA based cells are given in Figure 3(b) and (c). An equivalent circuit is employed to fit the tested data, see the inset of Figure 3(b). Generally, the high frequency arc is attributed to the hole diffusion in HTM, whereas the lower frequency part is determined by the electron recombination from the mesoporous TiO_2 with holes in the HTM, modeled by a recombination resistance (R_{rec}) [5]. To the same device, R_{rec} drops with the increasing forward bias voltage, mainly because the Fermi level of the mesoscopic TiO_2 is elevated at the forward bias which is beneficial for the electron flow across the TiO_2/$CH_3NH_3PbI_3$ interface [17]. Figure 3(d) shows the relationship between R_{rec} and applied bias voltages for the two devices. We can see that, for each HTM sample, as the bias voltages increasing linearly, the R_{rec} decreases exponentially, which is in good agreement with the reported work [5]. On the whole, for the two PSCs based on BPZTPA and MeO-BPZTPA, their tendency of R_{rec} is similar in the applied bias voltage range, indicating that similar recombination occurs at the interfaces of the two perovskite solar cells, as shown in Figure 3(d).

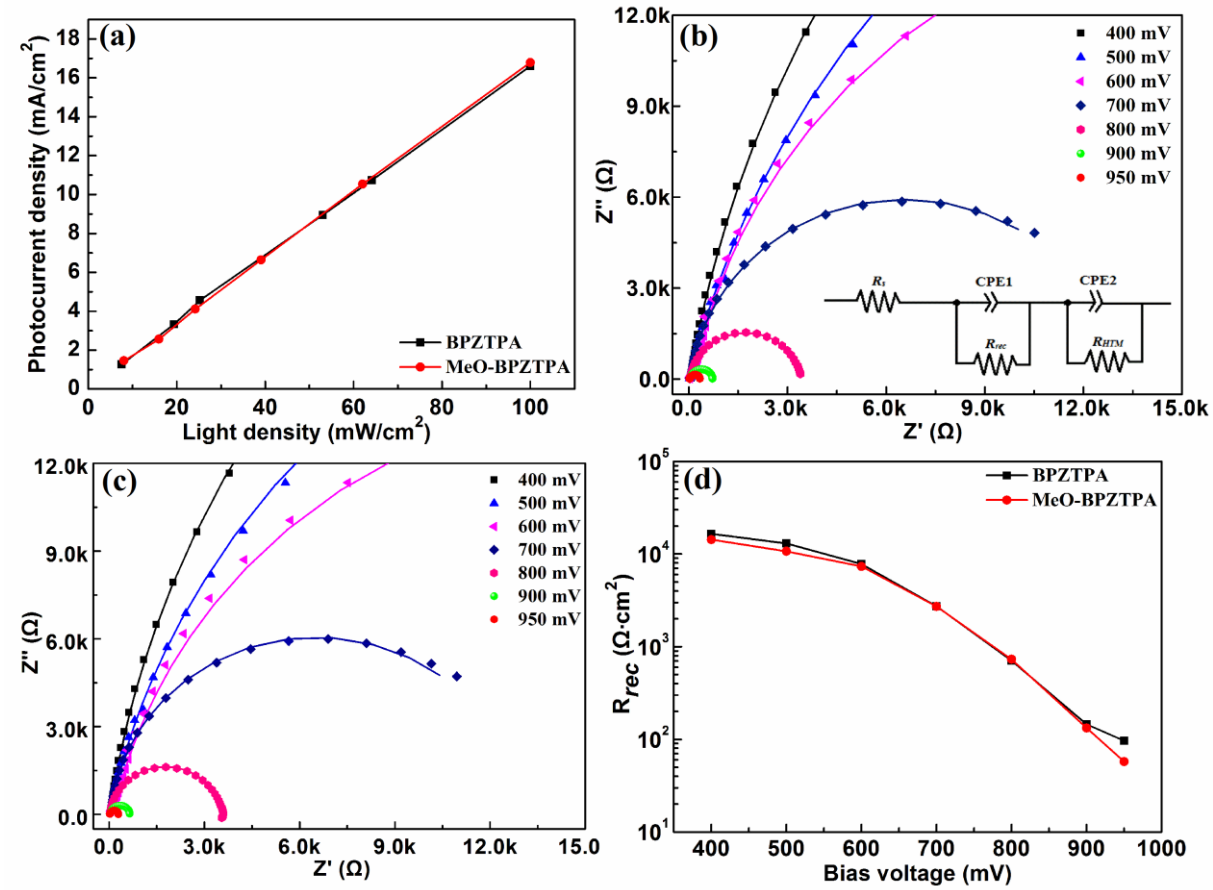

Figure 3. (a) The relationship of the J_{sc} of the HTM-based device with different light densities, (b) nyquist plots of the devices with BPZTPA layer measured at a bias potential from 400 to 950 mV in dark conditions (Inset: Equivalent circuit for fitting curves), (c) nyquist plots of the devices with MeO-BPZTPA layer measured at bias potential from 400 to 950 mV in dark conditions, (d) plots of R_{rec} vs bias voltages for the devices with BPZTPA and MeO-BPZTPA.

3.2.3. The influence of different HTM concentrations

The MeO-BPZTPA is taken as a model HTM to further investigate the influence of HTM thickness by different HTM concentration on the cell performance. As shown in †ESI Fig. S10 and Table 3, the cell fabricated at low HTM concentration (5 mg/mL) exhibits the worse photovoltaic performance. This could be attributed to the effective ohmic contact is difficult to be constructed at the interface between the metal and *p*-type semiconductor because of the very thin hole-transporting layer [27]. The better device performance is achieved as the HTM concentration is 10 mg/mL. As the HTM concentration much higher, the V_{oc} of devices has a slight drop, leading to a worse cell performance. This could be attributed to the elevated series resistance caused by the increased hole-transporting layer thickness at higher concentration [17]. This result proves that suitable hole-transporting layer thickness has strong impact on the cell performance.

Table 3. Photovoltaic parameters of perovskite solar cells based on different MeO-BPZTPA concentration.

Concentration (mg/mL)	J_{sc} (mA/cm^2)	V_{oc} (mV)	FF	PCE (%)
5	15.15	875.3	0.694	9.20
10	16.89	917.1	0.669	10.36
15	15.98	885.7	0.665	9.42
20	15.93	896.2	0.674	9.62

4. Conclusions

In summary, two phenonaphthazine derivatives (BPZTPA and MeO-BPZTPA) are successfully synthesized by a simple process. The compounds show high thermal stabilities, suitable HOMO levels and high hole mobilities. The perovskite solar cells based on MeO-BPZTPA as a HTM give an overall conversion efficiency of 10.36%, which is much higher than the cell without HTM. This result provides a new method to adjust molecular for the first time that *N*-heterocycle can be used as unit core, offering a new design strategy out of heterocyclic thiophene.

Acknowledgments

The authors gratefully acknowledge the financial support from National High-tech R&D Program (863 Program) (2015AA033402), the Science and Technology Planning Project of Tianjin Province, China (No. 14TXGCCX00017), Tianjin science and technology plan projects (13ZCZDGX00900) and the National Natural Science Foundation of China (No. 11474333).

Reference

[1] A. Kojima, K. Teshima, Y. Shirai, T. Miyasaka, J. Am. Chem. Soc. 131(17)(2009)6050-6051.

[2] Z. Yu, L.C. Sun, Adv. Energy Mater. 5(12)(2015)1500213-1500229.

[3] P. Ganesan, K.W. Fu, P. Gao, I. Raabe, K. Schenk, R. Scopelliti, J.S. Luo, L.H. Wong, M. Grätzel, M.K. Nazeeruddin, Energy Environ. Sci. 8(7)(2015)1986-1991.

[4] W.S. Yang, J.H. Noh, N.J. Jeon, Y.C. Kim, S. Ryu, J. Seo, S.I. Seok, Science, 348(2015)1234-1237.

[5] S.T. Lv, Y.K. Song, J.Y. Xiao, L.F. Zhu, J.J. Shi, H.Y. Wei, Y.Z. Xu, J. Dong, X. Xu, S.R. Wang, Y. Xiao, Y.H. Luo, D.M. Li, X.G. Li, Q.B. Meng, Electrochim. Acta. 182(2015)733-741.

[6] L.L. Zheng, Y.H. Chung, Y.Z. Ma, L.P. Zhang, L.X. Xiao, Z.J. Chen, S.F. Wang, B. Qu, Q.H. Gong, Chem. Commun. 50(2014)11196-11199.

[7] J.Y. Xiao, L.Y. Han, L.F. Zhu, S.T. Lv, J.J. Shi, H.Y. Wei, Y.Z. Xu, J. Dong, X. Xu, Y. Xiao, D.M. Li, S.R. Wang, Y.H. Luo, X.G. Li, Q.B. Meng, RSC Adv. 4(2014)32918-32923.

[8] Y.S. Liu, Q. Chen, H.S. Duan, H.P. Zhou, Y. Yang, H.J. Chen, S. Luo, T.B. Song, L.T. Dou, Z.R. Hong, Y. Yang, J. Mater. Chem. A, 3(2015)11940-11947.

[9] H. Choi, J.W. Cho, M. S. Kang, J. Ko, Chem. Commun. 51(2015)9305-9308.

[10] M.L. Petrus, T. Bein, T.J. Dingemans, P. Docampo, J. Mater. Chem. A, 3(2015)12159-12162.

[11] T. Krishnamoorthy, K.W. Fu, P.P. Boix, H.R. Li, T.M. Koh, W.L. Leong, S. Powar, A. Grimsdale, M. Grätzel, N. Mathews, S.G. Mhaisalkar, J. Mater. Chem. A, 2(18)(2014)6305-6309.

[12] A. Krishna, D. Sabba, H.R. Li, J. Yin, P.P. Boix, C. Soci, S.G. Mhaisalkar, A.C. Grimsdale, Chem. Sci. 5(7)(2014)2702-2709.

[13] H. Choi, S. Paek, N. Lim, Y.H. Lee, M.K. Nazeeruddin, J. Ko, Chem. Eur. J. 20(35)(2014)10894-10899.

[14] H.R. Li, K.W. Fu, P.P. Boix, L.H. Wong, A. Hagfeldt, M. Grätzel, S.G. Mhaisalkar, A.C. Grimsdale, ChemSusChem, 7(12)(2014)3420-3425.

[15] L.F. Zhu, J.Y. Xiao, J.J. Shi, J.J. Wang, S.T. Lv, Y.Z. Xu, Y.H. Luo, Y. Xiao, S.R. Wang, Q.B. Meng, X.G. Li, D.M. Li, Nano Res. 8(4)(2015)1116-1127.

[16] Y.K. Song, S.T. Lv, X.C. Liu, X.G. Li, S.R. Wang, H.Y. Wei, D.M. Li, Y. Xiao, Q.B. Meng, Chem. Commun. 50(2014)15239-15242.

[17] S.T. Lv, L.Y. Han, J.Y. Xiao, L.F. Zhu, J.J. Shi, H.Y. Wei, Y.Z. Xu, J. Dong, X. Xu, D.M. Li, S.R. Wang, Y.H. Luo, Q.B. Meng, X.G. Li, Chem. Commun. 50(2014)6931-6934.

[18] J.J. Wang, S.R. Wang, X.G. Li, L.F. Zhu, Q.B. Meng, Y. Xiao, D.M. Li, Chem. Commun. 50(44)(2014)5829-5832.

[19] M. Cheng, C. Chen, X.C. Yang, J. Huang, F.G. Zhang, B. Xu, L.C. Sun, Chem. Mater. 27(5)(2015)1808-1814.

[20] J.H. Im, C.R. Lee, J.W. Lee, S.W. Park, N. G. Park, Nanoscale, 3(10)(2011)4088-4093.

[21] H.S. Kim, C.R. Lee, J.H. Im, K.B. Lee, T. Moehl, A. Marchioro, S.J. Moon, H.B. Robin, J.H. Yum, J.E. Moser, M. Grätzel, N. G. Park, Sci. Rep. 2(2012)591.

[22] J.J. Shi, Y.H. Luo, H.Y. Wei, J.H. Luo, J. Dong, S.T. Lv, J.Y. Xiao, Y.Z. Xu, L.F. Zhu, X. Xu, H.J. Wu, D.M. Li, Q.B. Meng, ACS Appl. Mater. Interfaces, 6(12)(2014)9711-9718.

[23] V. Mimaite, J. Ostrauskaite, D. Gudeika, J.V. Grazulevicius, V. Jankauskas, Synth. Met. 161(2011)1575-1581.

[24] F. Zhang, S.R. Wang, X.G. Li, Y. Xiao, Curr. Nanosci. 12(2)(2016)137-156.

[25] S. Kazim, F.J. Ramos, P. Gao, M.K. Nazeeruddin, M. Grätzel, S. Ahmad, Energy Environ. Sci. 8(6)(2015)1816-1823.

[26] W.J. Chi, Q.S. Li, Z.S. Li, J. Phys. Chem. C. 119(2015)8584-8590.

[27] Y.Z. Xu, J.J. Shi, S.T. Lv, L.F. Zhu, J. Dong, H.J. Wu, Y. Xiao, Y.H. Luo, S.R. Wang, D.M. Li, X.G. Li, Q.B. Meng, ACS Appl. Mater. Interfaces, 6(8)(2014)5651-5656.